ABSTRACT

Title of thesis: Hot Electron Injection into Uniaxially Strained Silicon

Hyun Soo Kim, Master of Science, 2013

Thesis directed by: Professor Ian Appelbaum
Department of Physics

In semiconductor spintronics, silicon attracts great attention due to its long electron spin lifetime. Silicon is also one of the most commonly used semiconductor in microelectronics industry. The spin relaxation process of diamond crystal structure such as silicon is dominated by Elliot-Yafet mechanism. Yafet predicts the spin relaxation rate is related to temperature by the power law, $\sim T^{\frac{5}{2}}$, assuming that intravalley scattering is dominant. The conduction electron spin lifetime measured by electron spin resonance measurements and electronic measurements using ballistic hot electron method agrees well with Yafets theory. However, recent theory predicts a strong contribution of the intervalley scattering process such as f-process in silicon. The conduction band minimum is close the Brillouin zone edge X point, which causes strong spin mixing at the conduction band. A recent experiment of electric field-induced hot electron spin relaxation also shows the strong effect of f-process in silicon. In uniaxially strained silicon along crystal axis [100], it is predicted that the suppression of f-process leads to enhanced electron spin lifetime. By inducing a change in crystal structure via [100] uniaxial strain, the six fold degeneracy in

silicon becomes a two fold degeneracy, which is known as valley splitting. As the valley splitting increases, the intervalley scattering is reduced, which increases electron spin lifetime by a factor of four in 0.5% uniaxially strained silicon, according to recent theory.

In this thesis, we demonstrate ballistic hot electron injection into silicon under varying uniaxial strain. Spin polarized hot electron injection under strain is experimentally one of the most challenging parts of measuring conduction electron spin lifetime in silicon. Hot electron injection makes use of a tunnel junction, which is a thin oxide layer between two conducting materials. The two conducting materials are only tens of nanometers and the thin oxide layer is only a few $\AA$, so 0.5% strain on silicon along [100] axis can easily destroy thin films on the silicon substrate. In order to confirm the performance of tunnel junction, we use spin polarized hot electron injection method. The tunnel junctions consist of two kinds of ferromagnetic metals, normal metals and an oxide layer as tunnel barrier in order to measure the spin valve effect in silicon. Using silicon as a collector with a Schottky barrier interface between the metal and silicon, ballistic hot spin polarized electron injection into silicon is demonstrated. We also observed a change of the coercive field and magnetoresistance due to modification of local states in ferromagnetic metals and surface states at the interface between metal and silicon due to strain.

Hot Electron Injection
into Uniaxially Strained Silicon

by

Hyun Soo Kim

Thesis submitted to the Faculty of the Graduate School of the
University of Maryland, College Park in partial fulfillment
of the requirements for the degree of
Master of Science
2013

Advisory Committee:
Professor Ian Appelbaum, Chair/Advisor
Professor Isaak D Mayergoyz
Professor John Melngailis

© Copyright by
Hyun Soo Kim
2013

Table of Contents

1 Introduction 1
1.1 Semiconductor spintronics 1
1.2 Scattering processes 2
1.3 Strained Silicon 4
1.4 Ballistic hot electron injection 7
1.5 Spin polarization measurement 9
1.5.1 Spin Polarization 9
1.5.2 Spin lifetime measurement 10
1.6 Electron-field induced hot electron spin relaxation 11

2 Device Fabrication and Measurement Apparatus 15
2.1 Strain probe 15
2.2 Strain gauge 19
2.3 Design and fabrication of spin transporting silicon devices 20
2.3.1 3 Terminal device & electrode 20
2.3.2 4 Terminal device & electrode 25

3 Experimental Results 30
3.1 3 Terminal tunnel junction device 30

4 Conclusion 43

Bibliography 45

Chapter 1: Introduction

1.1 Semiconductor spintronics

Silicon CMOS devices are now getting close to their limits in the performance and size. In recent years, these limits have led worldwide attention to a new technology, semiconductor spintronics, which uses the electron spin in semiconductors. Spintronics has great advantages such as non-volatility and low power consumption for magnetic storage devices. Spintronics also has potential for quantum information processing which is the study of the quantum nature [1], [2].

In semiconductor spintronics, silicon is one of the most promising candidates. Silicon is already widely used material in existing devices. Silicon has the weak spin-orbit interaction, degenerate spin states, and zero hyperfine coupling. These properties give silicon a long electron spin lifetime, which makes it as the most promising material for semiconductor spintronics [4], [5], [6]. Previous experiments have shown that this long spin lifetime in bulk silicon. The goal of this thesis is to enhance electron spin lifetime in silicon by reducing one of the electron phonon scattering processes. The following sections in this chapter introduce the theoretical background of this thesis.

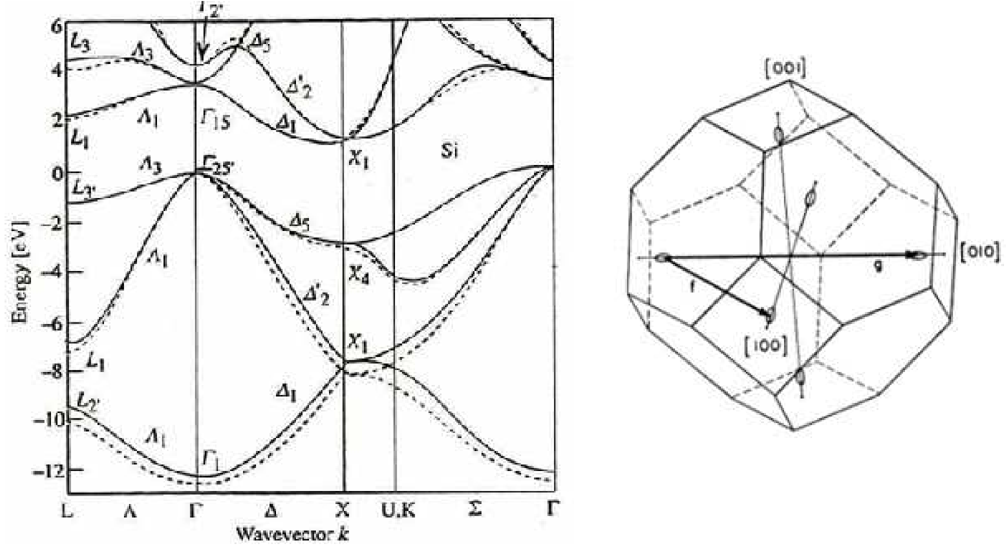

Figure 1.1: (a) Band structure of silicon calculated by pseudopotential technique [3]. (b) Brillouin zone of silicon, the two arrows between ellipsoids represent the f-process and g-process of intervalley scattering.

1.2 Scattering processes

The spin relaxation process in a diamond crystal structure such as silicon is dominated by the Elliot-Yafet mechanism, in which spins relax due to the momentum scattering by spin-orbit interaction [5], [7], [8]. Silicon has an indirect band gap due to its diamond structure. The minimum of the conduction band is located near the X-point, so there are six equivalent conduction band minima on crystal axis. In k-space, there are six constant energy surfaces, with two ellipsoids on each axis in k-space. There are two scattering processes related to these six ellipsoids: intervalley scattering and intravalley scattering [9]. In multivalley semiconductors, the intravalley scattering happens within one ellipsoid. In the intervalley scattering, the electron scatters from one valley to another valley. There are two types of intervalley

scattering: the f-process, in which electrons shown in Fig. 1.1 are scattered between ellipsoids that are sitting on the perpendicular axes, and the g-process, in which electrons are scattered between the ellipsoids on the same axis [10]. Because silicon is a multivalley semiconductors,Eliiot-Yafet mechanism is more effective since the multivalleys allows large momentum scattering. Due to the spin-orbit interaction and the inversion symmetry of silicon, the Bloch states are a mixture of Pauli spin up and spin down states [11]. By Fermi's golden selection rule, the spin scattering rate is proportional to the squared norm of the matrix element that couples spin up and spin down. Spin lifetime, τ_s is proportional to momentum relaxation time τ_p, by the relation, $1/\tau_s \sim |b|^2/\tau_p$, where the spin mixing probability, $|b|^2$, in silicon is 10^{-5}. Therefore, the spin relaxation time is longer than the momentum relaxation time [12], [13].

Yafet explained the temperature dependent spin relaxation rate with a power law of $T^{\frac{5}{2}}$ by assuming that the intravalley electron phonon scattering is the dominant spin relaxation mechanism in silicon [8]. However, a recent theoretical study predicts that a large contribution of f-process intervalley scattering due to the strong spin mixing at Brillouin zone edge, X point [14]. Two conduction bands with different spin states cross at the X point, where the absolute minimum of the conduction band is located. Therefore, f-process intervalley scattering contributes to the spin relaxation process significantly, which has been shown in recent experiment [14], [15]. In this study, electric field-induced hot electron spin relaxation is observed [15]. The valleys on the axis parallel to the electric field have larger effective mass compared to the valleys on the axes perpendicular to the electric field. The valleys with smaller

effective mass gains higher energy than other valleys with larger effective mass [11]. This induces more f-process intervalley scattering in order to achieve thermal equilibrium between the valleys. A more detailed explanation of this experiment is in section 1.6.

1.3 Strained Silicon

As MOSFET approaches their size limits, the enhancement of their mobility has gained attention to improve the performance. Application of uniaxial or biaxial strain to a MOSFET introduces a small change in a crystal structure. The change in the crystal structure leads to a change of the band structure of silicon [16]. Therefore, the strain induces a change in the band gap and effective mass in silicon [17], [18]. The mobility is also enhanced by the change of the effective mass which can improve the performance of MOSFET silicon devices.

Another interesting change occurs at the conduction band. Without strain, the six valleys in the k-space have the same energies. However, if uniaxial compressive strain is applied along the one of the crystal axes such as the [100] axis, the two valleys on [100] axis have higher effective mass, which leads to lower energy states compared to the four valleys that are perpendicular to [100] [16]. Fig. 1.2 shows the change of isoenergetic surfaces of valleys due to strain. The bigger ellipsoids represent the higher energy states. Therefore, the six fold valley degeneracy becomes two-fold degeneracy. This leads to the conduction band valley splitting, which reduces f-process intervalley scattering [16], [19]. Multi-valley semiconductors such as

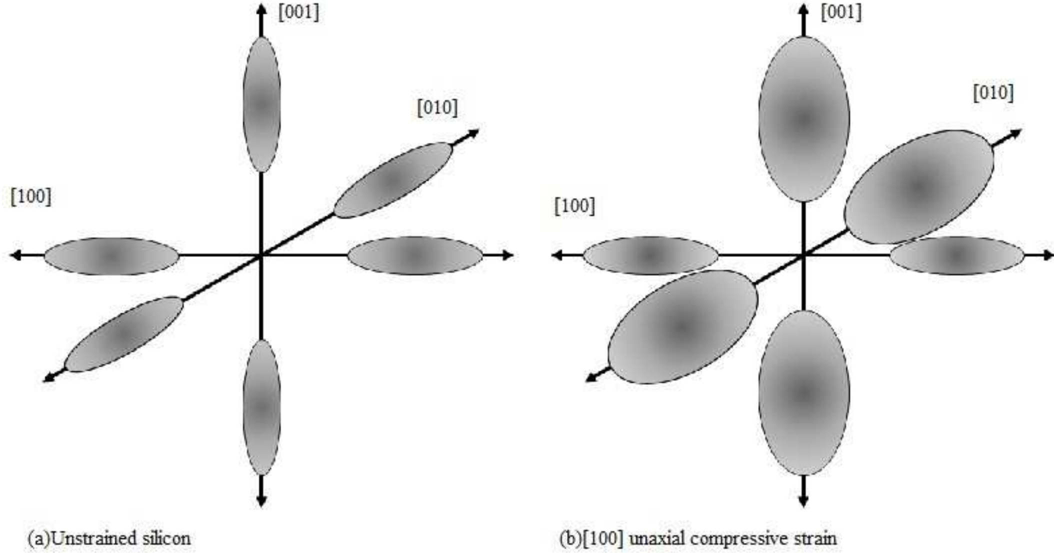

Figure 1.2: (a)The six valley structure of the conduction band in bulk silicon. (b)Uniaxial strain is applied in the [100] direction. Two ellipoids on [100] axis have lower energy states than the other four ellipoids on [010] and [001].

silicon allow the low energy scattering via large momenta [20]. As the splittings get higher, since the intervalley scattering is due to the electron phonon scattering, the transition between the valleys by electron phonon scattering is reduced [21]. The reduction of the intervalley scattering can increase the electron mobility since the intervalley scattering contributes significantly to the total scattering rate [16], [19].

In order to achieve longer coherent electron spin lifetime, in quantum computing, strain-induced valley splitting and degeneracy lifting are being studied [23]. As recent theoretical studies and experimental results show the large contribution of the intervalley scattering to spin relaxation in bulk silicon, the reduction of the intervalley scattering can reduce the spin relaxation rate. [14], [15] By applying uniaxial strain to silicon, the suppression of the intervalley scattering can be induced.

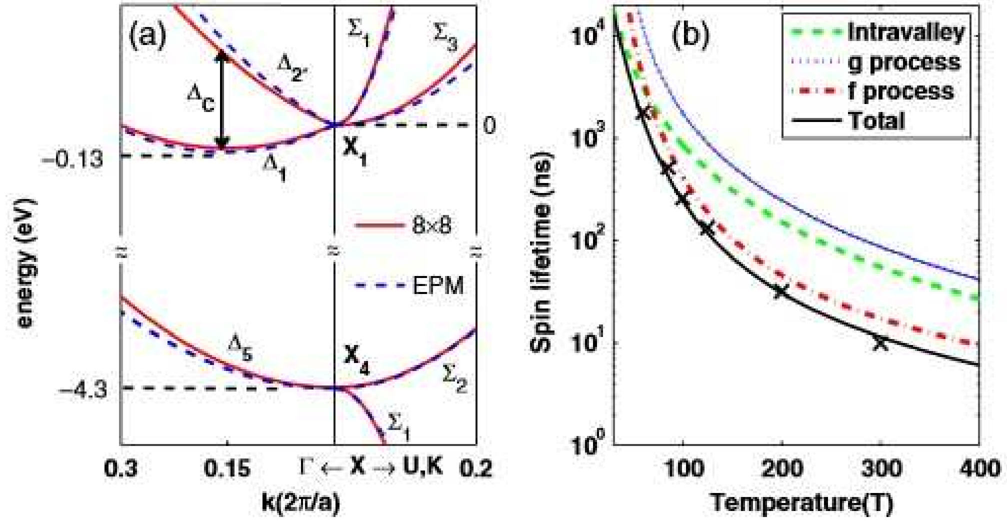

Figure 1.3: (a) Calculated band structure near the X point in silicon. The wave vector origin is taken at the X point where a $=5.43\mathring{A}$ is the lattice constant. Dashed(solid)lines are results of an empirical pseudopotential model 8×8 Hamiltonian [14].(b)Calculated spin relaxation time in silicon and contributions from intravalley, g-process, and f-process electron phonon interaction at high temperatures. The × symbols denote experimental results [14].

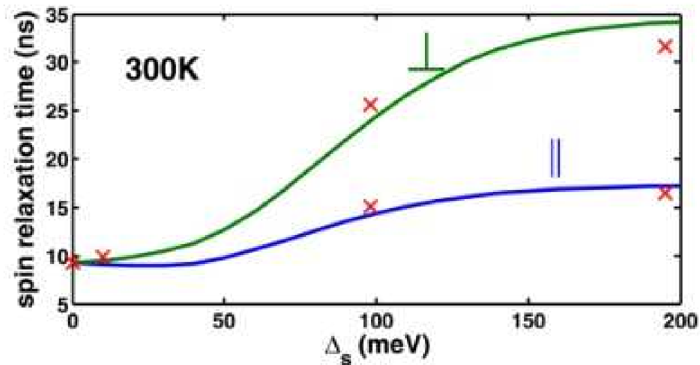

Figure 1.4: Calculated spin relaxation time in silicon versus valley splitting energy. The curve with a symbol, ($\perp$) shows the spin lifetime when the spin-quantization axis is perpendicular(parallel) to the valleys of lower energy [22].

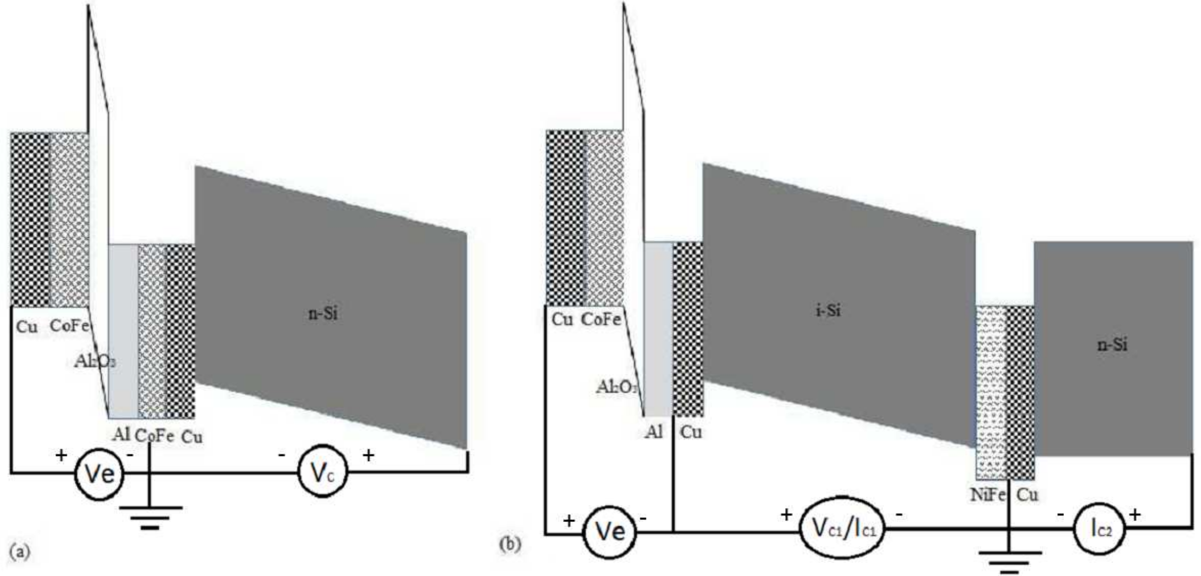

Figure 1.5: (a) 3 terminal device of a tunnel junction on n-Si for hot electron injection measurement. (b) 4 terminal device for spin life time measurement of silicon.

A theoretical study predicts a four-fold enhancement of spin lifetime in silicon with nearly 1% strain, which corresponds to $\sim 200meV$ splitting as shown in Fig. 1.4 [22]. The uniaxially strained silicon corresponds to the curve with a symbol $\times$ in Fig. 1.4.

1.4 Ballistic hot electron injection

In order to observe the spin orbit interaction in silicon, spin polarized current has to be injected into silicon. Electrical measurements of spin polarized electrons in silicon was demonstrated by using ballistic spin filtering effect [24]. A tunnel junction can work as a spin injector, by sandwiching a thin oxide layer between two ferromagnetic layers, which acts as the cathode and anode. Fig.1.5 shows a schematic of the band diagram of the devices.

The first device is a tunnel junction of ferromagnetic metals on an n-type silicon substrate and the second device is a device for measuring spin lifetime with the spin valve effect across an intinsic silicon substrate. The more details of each device will be explained in the next chapter. The electrons flow from the left to the right. In this section, we explain ballistic hot electron injection based on Fig. 1.5(b), since this is the device used to measure spin lifetime in silicon. As the voltage bias, V_e is applied between two metal layers, the spin polarized electrons tunnel through a ferromagnetic layer(CoFe) layer and the oxide layer. The tunneling current, I_e flows into a metal anode(Al/Cu). The energy of the spin polarized electrons tunneling through an oxide layer depends on V_e. This tunnel junction is deposited on an i-Si substrate, which is used as a transport layer. The metal-semiconductor interface forms a Schottky interface. The ballistic hot electrons travels through the anode. As the Fermi level of the hot electrons of the cathode by applying V_e becomes higher, the ballistic hot electrons travel into the conduction band of the silicon, where they quickly relax to the conduction band minimum. These injected hot electrons, I_{C1} travel through silicon via a drift and diffusion by the electric field applied across the i-Si. In order to detect the electron spin states at the end of the i-Si transport layer, we again employ the ballistic hot electron technique. This detecting technique requires a unique wafer bonding process, which i-Si wafer is bonded to another n-Si wafer. With thin metal layers including a ferromagnetic metal in between, due to the Schottky barrier between the i-Si and the ferromagnetic layer at the end of the transport layer, the hot spin polarized electrons, I_{C2} are injected from the i-Si into n-Si.

However, at room temperature, there exists a thermal current from the metal and silicon interface, also called a saturation current in a diode equation, that contributes to I_{C1} and I_{C2}. The saturation current is not spin polarized, so it is a noise signal for spin current measurements. Therefore, in order to reduce the exponentially temperature dependent saturation current, the experiment needs to be measured at low temperature.

1.5 Spin polarization measurement

1.5.1 Spin Polarization

Spin polarization is the degree to which the spin of electrons in the conduction band is aligned with a given direction. Once the spin of the electron is polarized, the densities of spin up electrons and spin down electrons are different [25].

In ferromagnetic metals magnetized in a given direction, the mean free path(mfp) for the electrons depends on the electron spin states. The mfp for spin up and spin down in a ferromagnetic metal is different. When the electron spin state is parallel to the direction of magnetization of a ferromagnetic metal, the mfp is longer than when the spin state is antiparallel [12]. In our device, there are two different ferromagnetic metals in the injector and the detector. By applying external magnetic field, the direction of magnetization of the ferromagnetic metals in injector and detector can be changed. Since there are two different ferromagnetic metals with different coercive fields, by changing the magnetization directions of the ferromagnetic metals in the injector and the detector to be parallel or anti-parallel to each other, the hot

spin polarized injected current in silicon can be filtered by the ferromagnetic metal in the detector. The change of the spin current in a detector determines the spin polarization.

$$P = \frac{I_P - I_{AP}}{I_P + I_{AP}} \tag{1.1}$$

where P is spin polarization, I_P is the current at the detector in a case of the magnetization of ferromagnetic layers in the injector and the detector are parallel, and I_{AP} in case of anti-parallel magnetization.

1.5.2 Spin lifetime measurement

Spin lifetime in silicon is measured between 60-150K by using a hot electron technique [24]. The spin lifetime is extracted from the spin valve measurement and spin transit time measurement. The spin valve effect is the measurement of spin polarization with a hot electron technique as above. The spin transit time is the traveling time of electrons in silicon. The various transit times, t, can be measured by changing the bias voltage across a transport i-Si. Spin lifetime is fitted with the equation, $P(t) = P_0 e^{-\frac{t}{\tau_s}}$ [26], where P_0 is a fitting parameter. The temperature dependence of spin lifetime predicted by Yafet, $\sim T^{-\frac{5}{2}}$ agrees with the experimental results [8]. For our experiment, by using the same hot electron technique and the exponential decaying equation of spin polarization, the change of spin lifetime in i-Si can be measured. In the following chapter, the methods used to apply the uniaxial strain on the device and fabrication process of the devices are introduced.

1.6 Electron-field induced hot electron spin relaxation

A recent experiment shows strong f-process intervalley scattering in silicon induced by a strong electric field [15]. By Elliot-Yafet theory, the depolarization of spin polarized electrons in silicon depends only on the transit time across transport silicon layer. Therefore, as the transit time decreases, the spin polarization increases. In a low field regime, spin polarization increases as electron velocity increases. However, in a high field regime, this experiment shows the spin polarization decreases as electron velocity increases as shown in Fig. 1.6, which contradicts to the Elliot-Yafet theory. In a low field, the six conduction valleys have similar energy. However, in a high field regime, the repopulation between valleys are induced by the difference of the effective mass in valleys on different axes, which is known as Gunn effect [27], [28]. Fig. 1.6(b) shows decrease of polarization at short mean transit times, which means higher electric fields. Also, Fig. 1.7(c) shows that the accelerating voltage increases, polarization decreases [15].

Fig. 1.7(a) shows the Monte Carlo steady-state energy distributions in hot and cold valleys at 30 K and 4 kV/cm. Fig. 1.7(b) shows the repopulation ratio, n_c/n_h, where n_c is electron population in cold valleys and n_h is electron population in hot valleys. In Fig. 1.7(b), at intermediate fields the repopulation ratio is highest since electrons in hot valleys gain enough energy for intervalley scattering. However, at high fields, electrons in cold valleys also become energetic enough to scatter to other valleys. This causes more symmetric valley population reducing the repopulation ratio [15]. Hot electrons driven by an electric field gain enough energy to induce more

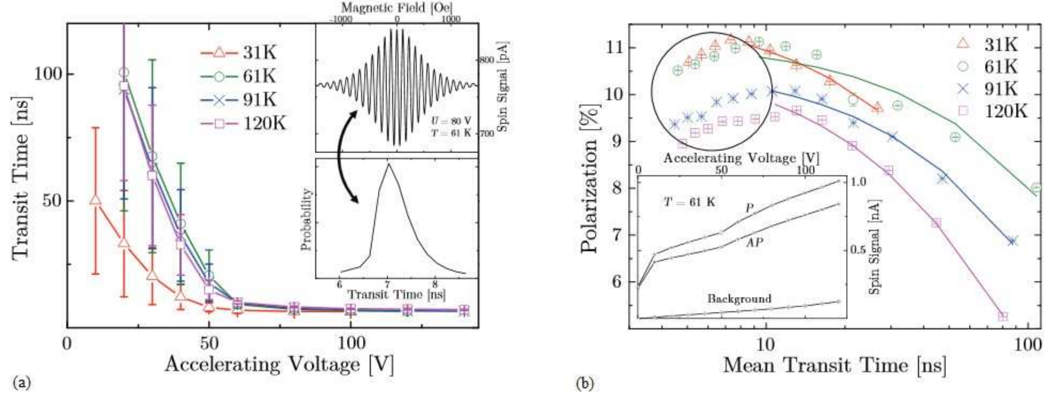

Figure 1.6: (a) Transit time across silicon as a function of accelerating voltage across silicon. Top inset: spin precession data 61K and 80V(3.5kV/cm). Bottom inset: transit time distribution obtained by transforming the precession signal. (b) Current polarization in a ferromagnet/silicon/ferromagnet device as a function of mean transit time. Inset: example spectroscopy at 61K in a parallel(P) and antiparallel(AP) magnetization configuration, with background signal subtraction [15].

intervalley electron-phonon scattering. As shown in Fig. 1.7 (d), the characteristic scale of V_0 for f-process induced spin depolarization is introduced from the equation, $P \sim P_0\left(1 - \frac{V}{V_0}\right)$, where V_0 is extracted from the data of Fig. 1.6. Fig. 1.7(c) and (d) also shows the agreement between the experimental results and the Monte-Carlo prediction. From this experiment, we can see depolarization effect caused by a strong f-process intervalley scattering that occurs to recover thermal equilibrium [15].

This experiment performs the spin valve measurement and spin precession measurement. The spin valve measurement is identical to the one explained in a previous section, which was performed to extract the polarization. The spin precession measurement is performed to extract the transit time of the spin current in silicon shown in Fig. 1.6. Electron spin is a magnetic momentum, so, it experiences

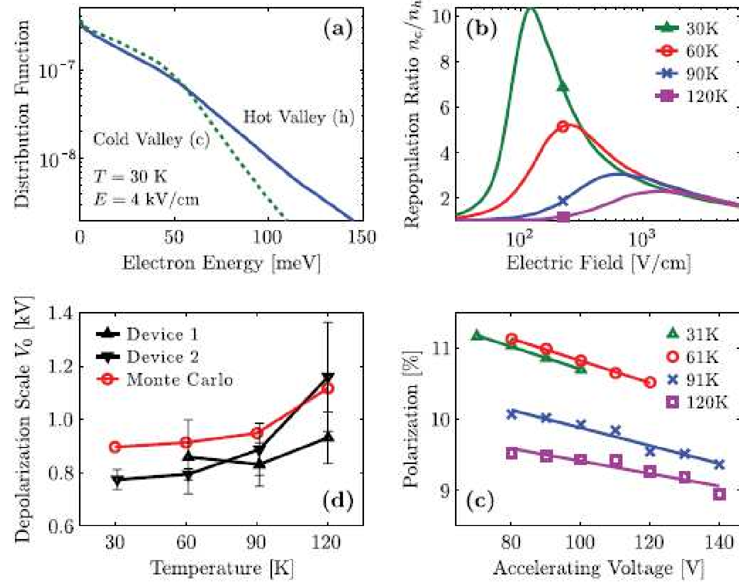

Figure 1.7: (a) Electron distribution hot (solid line) and cold (dashed line) valleys. The total electron density is 10^{12} cm^{-3}, the electric field is 4 kV/cm and the lattice temperature is 30 K. (b) Ratio between electron densities in cold and hot valleys as a function of the field. (c) Experimental depolarization at high-fiels(extracted from Fig.1.6). (d) Characteristic voltage scale for field-induced spin depolarization as a function of temperature. [15].

a torque in an external magnetic field. In a magnetic field perpendicular to the electron's spin axis, electron spin precess along the transport direction. The frequency of this precession, known as the Larmor frequency, is linearly proportional to the magnetic field and has the value, $\omega = \frac{g\mu_B B}{\hbar}$, where g is a g-factor, μ_B is the Bohr magneton, $\hbar$ is the reduced Plank constant, B is the external magnetic field. As shown in Fig. 1.6, the Fourier transform of the spin precession signal is the transit time distribution of spin electrons in silicon.

Chapter 2: Device Fabrication and Measurement Apparatus

2.1 Strain probe

The first key step of this experiment is to apply uniaxial pressure to the silicon along one of the crystal axes. In order to measure the spin lifetime, the hot electron injection technique requires the low temperature measurements to reduce the thermal current at the interface between the metal and silicon, so the probe for this experiment has to fit in a cryostat. Also, since we need to measure the change of the electron spin lifetime under various strains, we must have the capability to control the pressure on the silicon device. For this reason, the design of the probe adapts the design of a vise.

The key design of the probe is the component where the sample is mounted and the pressure is applied to the silicon along the crystal axis. In order to change the pressure, a micrometer head with non-rotating spindle is mounted above the sample. The motion of the micrometer head is one dimensional, which allows it to apply uniaxial pressure on the device. The micrometer head is mounted on an aluminum block, which is non-magnetic. To avoid the effect of stray field, it is important to use non-magnetic materials near the silicon sample. As shown in Fig. 2.2 the micrometer head holder has three parts: a body, a clamp, and a bottom.

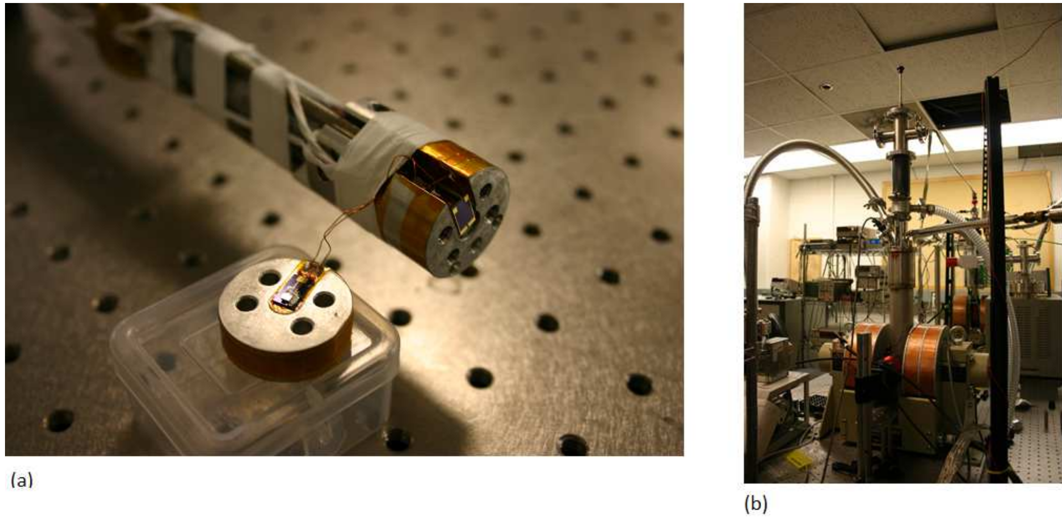

Figure 2.1: (a) A four terminal device sitting on the bottom electrode is mounted on bottom piece. The top electrode is mounted on the body. (b) Probe is mounted on a cryostat and a magnetic coils are aligned near the device.

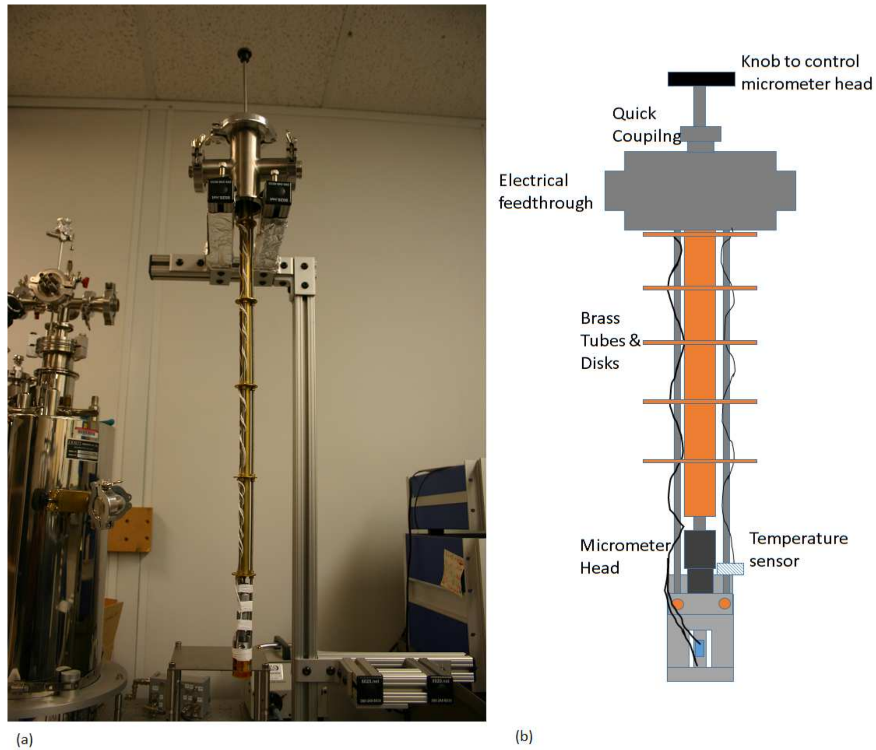

Figure 2.2: (a) Picture of strain probe. (b) Mechanical drawing of probe.

The micrometer head is mounted on the body of the aluminum holder with a clamp made of aluminum. The silicon sample sits on the bottom part of the holder. The bottom part is fixed on the body with four screws. There are three stainless steel rods attached to the holder. The other end of the rods are attached to the quick coupling on the top of the probe. The micrometer head is coupled with a long ,stainless steel rod, which is also coupled to the quick coupling on the top of the probe. At the end of this rod that allows the micrometer head to be rotated from the outside of the cryostat. The brass disks are placed along those three rods to support the holder, and brass tubes are inserted between the disks. When the pressure is applied, due to the torque on the holder from the micrometer head, the three rods are rotated. This rotation causes a displacement of the silicon sample in the external magnetic field. The brass tubes and disks hold the probe in the original shape. For the electrical connection, copper terminals on polyimide film are glued to the bottom piece.

Another important role of this probe is to measure the strain applied to the silicon. Since the thickness of the device is about 600 um, and the most commercially available strain gauges are much larger, direct measurement of the strain is very difficult. The alternative way to measure the strain is to measure the pressure at another point linearly coupled to the device between the device and the shaft of the micrometer head using a strain gauge. The aluminum rod and a ceramic with a quarter inch diameter are placed. The strain gauge is glued on the side of the aluminum rod. Since the aluminum rod is coupled with the micrometer head and the device, they experience the same force. Therefore, the pressure or stress, σ,

applied to the device can be calculated by a simple Young′s modulus, Y, which is the relationship of the stress, σ and the strain, ε. The strain is proportional to the stress through the relation, $\varepsilon = \frac{\sigma}{Y}$. From Young′s modulus relation, the strain on silicon can be extracted from the strain on the aluminum rod. Another consieration is that the pressure on the aluminum rod, σ_{Al} is different from the pressure on the device, ε_{Si} due to the difference in cross-sectional area. However, the rod and the device feel the same force from the micrometer head. The conversion of strain on the aluminum rod to strain on silicon is

$$\varepsilon_{Si} = \frac{\sigma_{Si}}{Y_{Si}}, \sigma_{Si} = \frac{F}{A_{Si}} \tag{2.1}$$

$$\varepsilon_{Al} = \frac{\sigma_{Al}}{Y_{Al}}, \sigma_{Al} = \frac{F}{A_{Al}} \tag{2.2}$$

$$\varepsilon_{Si} = \frac{\varepsilon_{Al} \times Y_{Al} \times A_{Al}}{Y_{Si} \times A_{Si}} \tag{2.3}$$

where ε_{Si} is the strain on silicon, ε_{Al} is the strain on the aluminum rod, F is the force applied on the rod and the device, σ_{Al} is the stress on the aluminum rod, σ_{Si} is the stress on a device, Y_{Al} is Young′s modulus of aluminum, Y_{Si} is Young′s modulus of silicon, A_{Al} is the cross-sectional area of the aluminum rod, and A_{Si} is the cross-sectional area of the device. At room temperature, Y_{Si} in [100] direction is 69 GPa at room temperature, but the temperature dependence of the Young′s modulus has to be accounted for since the experiments are at low temperature. The temperature dependence of Y_{Al} is approximately a fourth order polynomial function,

$$\begin{aligned} Y_{Al} &= -1.0709 \times 10^{-9} \times T^4 + 8.9936 \times 10^{-7} \times T^3 + \\ &\quad -2.9241 \times 10^{-4} \times T^2 + 0.01030636 \times T + 77.71221 \end{aligned} \tag{2.4}$$

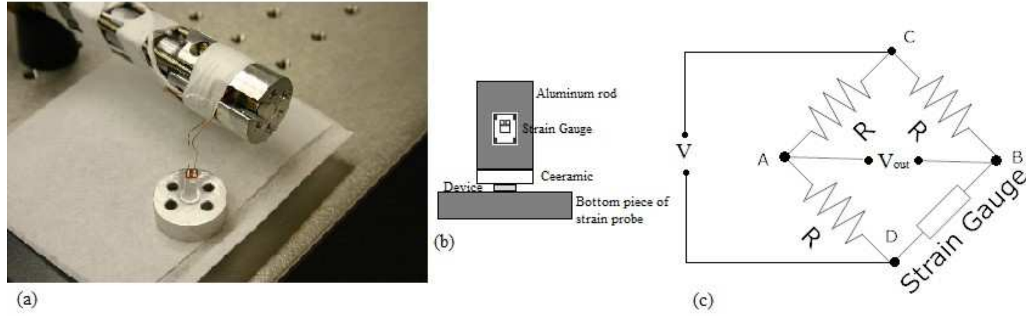

Figure 2.3: (a) Picture of the head part of a strain probe. (b) Schematic of the strain gauge and a device in a strain probe. (c) Wheatstone bridge circuit for a strain measurement with a strain gauge.

, where T is temperature in Kelvin [29]. The temperature dependence of Y_{Si} is nearly linear in the [100] direction, Young′s modulus changes $-78.8 \times 10^{-6} \frac{GPa}{C^{\circ}}$ [30].

2.2 Strain gauge

The strain gauge is a device that measures the strain on a material. As the material is deformed by the pressure, the strain gauge is also deformed. As the shape of the gauge changes, the pattern of the strain gauge is stretched or compressed, causing a change in its resistance. In a case of compression, the pattern of the strain gauge becomes thicker which reduces the resistance of the strain gauge. By measuring this change in the resistance, the strain of the material can be determined. Unfortunately, the change of the resistance is very small, so in order to measure it, the Wheatstone bridge circuit is adopted. The Wheatstone bridge circuit has been widely used for precise measurements of the unknown resistances. For the strain measurement, one of four symmetric resistors, as shown in Fig. 2.1(c), is replaced

with a strain gauge that has the same resistance as the other three precise resistors in the circuit. Constant dc voltage is applied between C and D in Fig. 2.1. When the four resistors of the Wheatstone bridge circuit are the same, the voltage drop, V_{out} across the A and B is zero in Fig. 2.1. The deformation of the strain gauge causes the change in the resistance of the strain gauge. The symmetry of the resistance is broken, and the voltage drop between A and B changes. Also, by taking into account the resistance of the cable and the temperature dependence of the strain gauge, we can measure the precise strain of the aluminum rod.

2.3 Design and fabrication of spin transporting silicon devices

2.3.1 3 Terminal device & electrode

The uniaxial pressure can also change the band structure of the silicon. In particular, the uniaxial compressive pressure splits the two conduction minimum bands, which is called valley splitting. The conduction band splitting, which increases the electron spin lifetime in silicon, also lowers the band gap by lowering the conduction minimum, and the change of Schottky barrier is correlated to the change of the band gap. In order to measure the Schottky barrier height of the silicon, the hot electron injection is used. By using a tunnel junction, which is comprised of two thin metal films with a thin oxide layer between them, the electrons can be injected into the silicon as shown in Fig. 1.5. When thin ferromagnetic films are used for the tunnel junction, by applying the external magnetic field in plane, the spin orientation of the electrons is aligned with respect to the magnetization

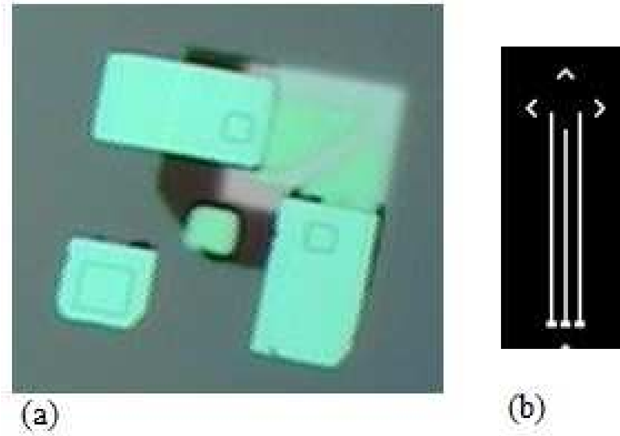

Figure 2.4: (a) Top View of a 3 terminal device. The two rectangles are electrical contacts for a tunnel junction. One square is for n-Si. (b) A drawing of the electrode. The two long lines on left and right sides are for a tunnel junction. A short line in the middle is for n-Si.

direction of the ferromagnetic films. By depositing two layers of ferromagnetic films separated by a thin oxide layer, the spin polarized current injection under pressure can be demonstrated.

The tunnel junction is made of layers of thin metal films, which are each only a few nanometer thick. The oxide layer of the tunnel junction is approximately a few angstroms thick. Even without pressure on the device, the oxide layer can be broken at around 1 volt at room temperature. The tunnel junction can be tested with a 3 terminal device if the tunnel junction can survive under pressure.

The hot electron injection requires a good Schottky contact between the semiconductor and the metal. The native oxide on the top of the silicon has to be carefully removed, through hydrofluoric acid(HF) etching. The metal depositions are performed in a ultra-high vacuum(UHV) chamber with an e-gun evaporator.

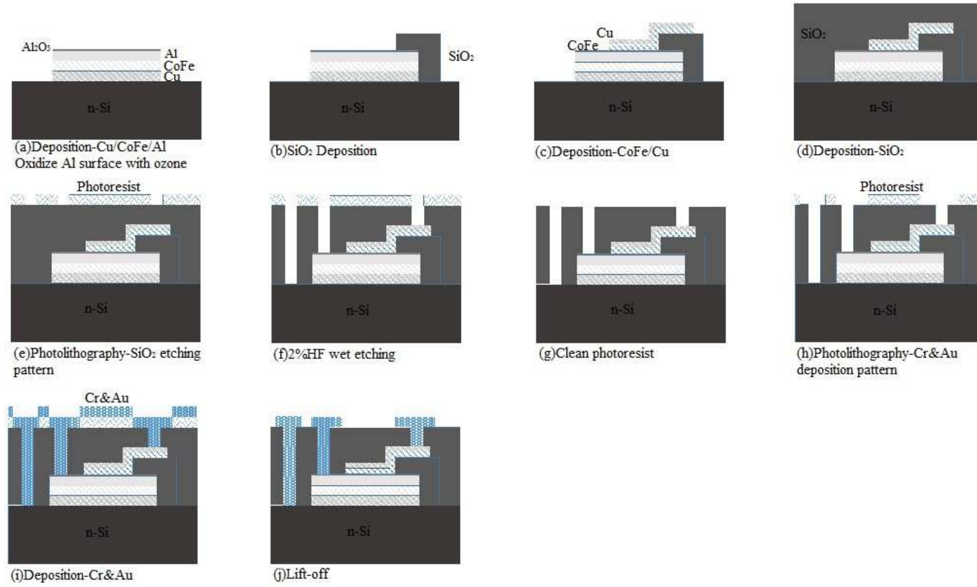

Figure 2.5: Fabrication process of 3 terminal device: (a) Deposition of the cathode(Cu/CoFe/Al) and oxidization of a top Al layer. (b) Deposition of SiO_2. (c) Deposition of the anode(CoFe/Cu). (d) Deposition of SiO_2. (e) Photolithography-patterning for wet etching. (f) 2% HF etching SiO_2. (g) Cleaning photoresist with solverns. (h) Photolithography-patterning for Cr/Au. (i) Deposition of Cr/Au. (j) Lift-off photoresist with acetone.

The fabrication process is explained in Fig. 2.5. Before any deposition on the silicon, the native SiO_2 layer on n-Si is etched with diluted 2% HF for 3 minutes. In Fig. 2.5 (a) thin layers of Cu(7nm), CoFe(7nm), and Al(8nm) are deposited with a square patterned shadow mask. After the deposition, the top Al layer is oxidized by ozone which is generated by UV light. (b)With a L-shaped shadow mask, an SiO_2(100nm) layer is deposited as a buffer layer. (c)Another two layers are deposited with two trapezoid shadow masks. A layer of CoFe(20nm) is deposited, and a layer of Cu(30nm) is deposited on top of CoFe. The CoFe layer with a right trapezoid pattern has a thickness twice the CoFe layer of a square pattern to create different coercive fields for each layer. The different coercive fields allow us to measure the spin valve effect. (d) A thick layer of SiO_2 is deposited on top of the tunnel junction to electrically protect the device from the metal layers of the electrodes. (e,f)Three square holes are etched in the SiO_2 with 2% diluted HF. Two squares are for two trapezoids of the cathodes, and the third square is for contacting the n-Si. (h)After etching, large squares on top of the etched areas are patterned with a photoligthography. (i,j)After depositing Cr(5nm) and Au(100nm), the unwanted Cr and Au is lifted off with acetone, methanol, and isopropyl alcohol.

However, the main challenge was to design electrodes to make electrical contacts. Since the device is surrounded by the probe, the wire bonding is not possible. Also, in order to measure the exact spin lifetime under pressure, the entire device has to be strained by the same amount, so the size of the device is constrained. Instead of increasing the size of the device, the electrodes are fabricated on a silicon wafer with a thermal oxide layer. Since the device has to be compressed, by putting

the electrodes between the probe and the device, they contact to each other firmly.

Another challenge is that once the tunnel junction on the n-Si and the electrodes on the other Si wafer are compressed together, the electrodes can also contact the other areas of the device. Therefore, the tunnel junction has to be insulated to all areas except the contact electrodes.

Since the electrodes and the device are making contacts by compression instead of wire bonding, all the electrical contacts for the device are designed on the top of the device. The device consists of two cathodes and one anode. The two cathodes are the right trapezoids, and the anode is a square shape. The tunneling barrier between the cathode and the anode is only a few angstroms thick. In this electrode design, there is no contact to the anode, by increasing the source current to one of two cathodes until breaking the tunneling barrier, one of cathodes makes ohmic contact to the anode. This broken cathode becomes the contact to the anode.

The electrodes are fabricated on a silicon wafer with a 200 nm thermally oxidized layer. After photolithography patterning, 5nm of Cr is deposited on top of the SiO_2 layer. 100nm of Au is deposited on top of the Cr layer. Cr is used as an adhesive layer for the Au layer on SiO_2. The excess Cr and Au layers are lifted off with acetone.

The electrode is mounted on the bottom piece of the probe with photoresist. The top side of the device, where the patterns of Au are deposited, is placed on top of the electrode, so, the device and the electrodes contact each other.

2.3.2 4 Terminal device & electrode

The spin transport silicon device used for the spin lifetime measurements has a 4 terminal configuration. For the 4 terminal device, the hot spin polarized electrons are injected into an i-Si. The electrons are transported through the i-Si wafer. At the end of this i-Si transport layer, the current is detected using hot electron injection into an n-Si as a detector. Between the transporting silicon and the detecting silicon, there are metal layers which include a ferromagnetic material. Therefore, two terminals for the tunnel junction, one terminal for the metal layer sandwiched between the two silicon wafers, and one terminal for the silicon detector compose the 4 terminal spin transport device.

The detector of the 4 terminal device also uses the hot electron injection, so, the quality of the Schottky interfaces between the bonded wafers and the metal layers are very important. The metal layers are deposited on the silicon wafers to help with adhesion of the wafers during the wafer-bonding process. The contaminants on the wafers can significantly reduce the bonding quality and the performance of the device. In order to minimize contaminations, the wafers are etched with 2% HF and carefully inspected. The wafers are bonded in a UHV chamber with a typical pressure of around 3×10^{-8}, which means that the contamination in the chamber is negligible.

The deposited metal layers are NiFe and Cu. The 4nm Cu layer is first deposited on the n-Si detector wafer, and The 2nm NiFe layer is deposited on both the n-Si detector and the i-Si transport. At the end of the NiFe deposition, the two

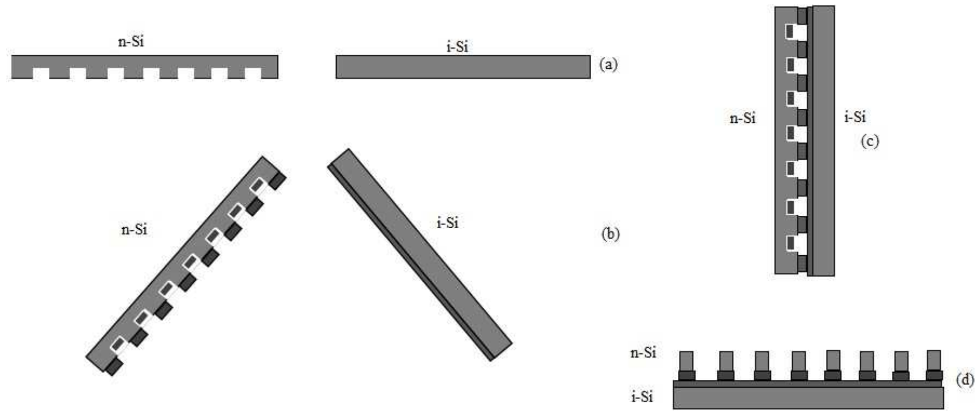

Figure 2.6: This is a schematic drawings of wafer bonding process. (a)n-Si has trench cuts on the bonding side before bonding. (b) During metal deposition which has darker color, two wafers are slowly brought together. (c) At the end of deposition, two wafers are compressed together. (d) After bonding, we cut the back side of n-Si in order to expose the buried metal layers between two wafers.

wafers are brought together and pressed by mechanical arms, which are controlled from the outside of the chamber.

Once it is bonded, it is difficult to make electrical contact to the buried metal layer between the two wafers. Therefore, before wafer bonding, we makes trench cuts into n-Si wafer. The top surface of the wafer is covered with a photoresist to protect it from the contamination during trenching. After making these trenches on the detector, the detector is thoroughly cleaned with solvents and wet etched with diluted 2% HF so that there are no contaminants left on the surface. After wafer bonding, in order to expose the buried metal layer, we also makes trenches on the back side of the detector along the trenches already on the buried metal side.

After the buried metal layers are exposed to make electrical contacts, the tun-

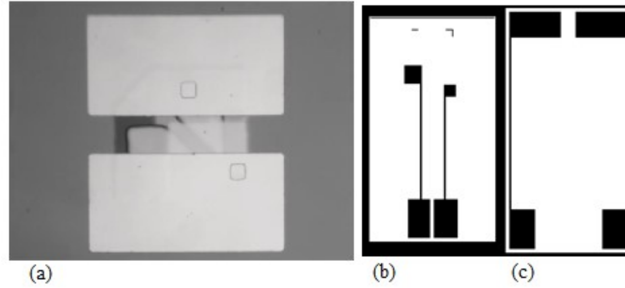

Figure 2.7: (a) Top view of 4 terminal device after lift-off process of Cr&Au layers. Top rectangle is a cathode and bottom one is an anode. (b) A drawing of a bottom electrode. The bottom electrode is for n-Si and a buried metal layer. (c) A drawing of top electrode. The top electrode is for a cathode and an anode.

nel junction is fabricated on the top surface of the transport silicon. The fabrication process of the tunnel junction is almost same as the 3 terminal device. Since electrical contact to the transport silicon is not necessary, the pattern of the Cr and Au layers on top of the SiO_2 is different. Two contacts are needed for the cathode and anode of the tunnel junctions, and the two contacts are needed onto the buried metal layer and the detecting wafer.

The tunnel junction of the 4 terminal device has the same patterns as the 3 terminal device. The anode is a square with the copper and aluminum layers. The L-shape pattern is for a thick SiO_2 layer. The trapezoid patterns for the cathode has CoFe and Cu layers. On the top of the tunnel junction, a 200nm SiO_2 layer is deposited. We etch two square patterns, one on the cathode and the other one on the anode, with diluted 2% HF. After wet etching, two large rectangles are patterned on top of two squares for Cr and Au deposition. After deposition of 5nm Cr and 100nm Au, we lift off the rectangle patterns of Cr and Au.

The 4 terminal device needs the electrical contacts at the top of the device, at the middle of the device which is the buried metal layer, and at the bottom which is the n-Si detector. In order to make 4 terminal electrical contacts, two separated electrodes are fabricated. One electrode is placed at the bottom of the device and the other electrode is sitting at the top of the device.

As shown in Fig. 2.7, the design of the bottom electrode is two lines, one is for the n-Si, and the other for the buried metal layer. We put a small amount of indium on the side of the n-Si for a good electrical contact. At the area where the device is sitting, there are two squares, which give more area to make electrical contacts to the n-Si and the buried metal layer. There are two L-shaped patterns to mark the position of the device. At the other end of the patterns, there are two large rectangles for wire bonding to the electrical terminals on the bottom piece of the probe. For good adhesion and electrical contact, we fix the device on the bottom electrode by putting silver paint on the indium contact and the bottom electrode. Since the buried metal layer and the bottom electrode are facing each other, we cannot wire bond the buried metal layer to the electrode, so we cut a thin aluminum wire for wire bonding. With silver paint, we glue the wire to the buried metal layer and the bottom electrode. There is kapton tape between the bottom electrode and the bottom piece of the probe. The kapton tape is a good insulator, so it protects the bottom electrode from being electrically shorted to the bottom piece of the probe. The bottom electrode is glued with photoresist on the top of the kapton tape.

Fig. 2.7(c) shows two large rectangles patterned at the place where the tunnel

junction anode and cathode of the device will contact. There are another two rectangles at the other end of the electrode for the wire bonding to the electrical terminals on the body of the probe. There are two lines to connect the sets of rectangles. When the device and both electrodes are mounted on the probe, the two electrodes are facing each other. The wires that are connected to the bottom and the body of the probe can touch each other and short the circuit. In order to avoid this shorting problem, the rectangles on the bottom electrode are placed at the center of the configuration and the rectangles on the top electrode are placed on the edge of the electrode. The electrical terminal on the body are on the side of the opened slot of the body so that we can connect the top electrode to the terminals on the body of the probe. In order to connect wires from the top electrode to the terminals on the body, before mounting the top electrode to the probe, we wire bond the top electrode and cut the other end of the wire with sufficient length to connect to the terminals on the body. After mounting the top electrode to the probe, the wires on the top electrode are glued on the terminals on the body with silver paint.

Chapter 3: Experimental Results

3.1 3 Terminal tunnel junction device

Before measuring spin lifetime in silicon with the 4 terminal device, we need to confirm that the probe can apply strain on a device without destroying it. The tunnel junction for the injector has a nanoscale thin metal films, and a thin Al_2O_3 tunnel barrier, between the cathode and the anode, which is only a few of angstroms thick. We were concerned that this thin tunneling barrier would not survive under about 1 GPa, so a 3 terminal device is designed to test the performance of a tunnel junction under strain. As explained in the first chapter, strain induces band gap narrowing in Si, which also causes Schottky barrier height (SBH) lowering at the interface between the anode and silicon. In the case of hydrostatic pressure on silicon, the band-gap changes 1.41meV per kbar [31]. The change of the band gap occurs at the conduction band minimum, therefore, this is a good approximation for the change of the SBH as a function of pressure [32].

With a hot electron method as described in Chapter 1, we can directly measure the SBH. When V_e is lower than the SBH, there is no hot electron injection since there is no available energy state in the band gap of the silicon for electrons to tunnel into. However, when V_e is higher than the SBH, ballistic hot electrons can be injected

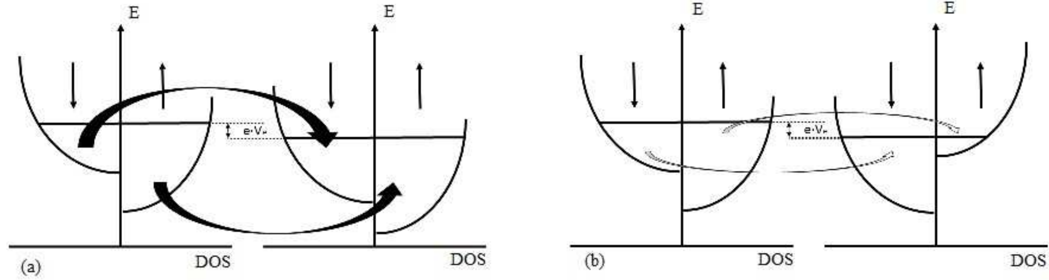

Figure 3.1: (a) This is when magnetizations are parallel. The left is cathode. The right is anode after applying V_e. The thick arrows indicates that more electrons tunnel through the barrier. The up and down arrows represent the spin up and down. x-axis is the densith of state(DOS), y-axis is energy. (b) This is when magnetizations are anti-parallel. Thinner arrows indicates fewer tunneling electrons.

into silicon and will quickly relax to the conduction band minima. This 3 terminal device consists of a tunnel junction with ferromagnetic metals in the cathode and anode [33]. Its structure resembles that of a magnetic tunnel junction (MTJ). In spintronics, MTJ is a well-studied device especially for MRAM [34]. An MTJ is a device with two ferromagnetic materials separated by a thin oxide layer. In an external magnetic field, MTJ acts as a spin filter using a tunneling effect. However, in our device, there are normal metals such as copper and aluminum in the anode and cathode, so even when an external magnetic field is applied, the tunneling current is not changed. As explained in Chapter 1, the spin valve measurement across silicon is required to extract the spin lifetime. The spin valve signal only comes from the spin filtering process of the tunnel junction. Therefore, the spin valve measurement of a tunnel junction on n-Si is proof of spin polarized hot electron injection into silicon.

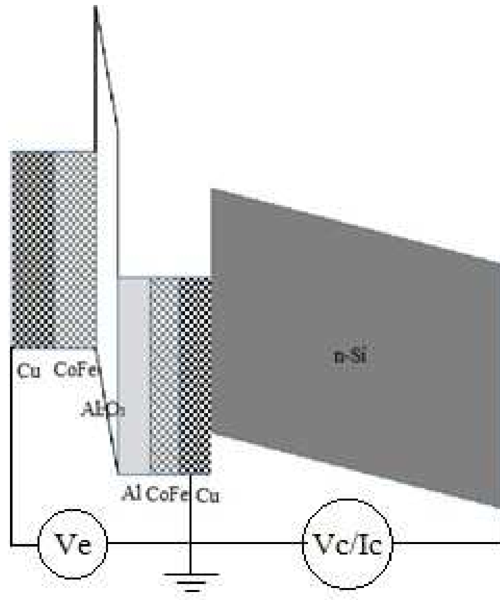

Figure 3.2: Band diagram of 3 terminal device. V_e is the emitter voltage across tunnel junction. V_C is collector voltage across n-Si. I_C is the collector current

In the anode, there are 7nm Cu, 7nm CoFe, and 8nm Al layers. In cathode, there are 20nm CoFe, 30nm Cu, 5nm Cr, and 100nm Au layers. The band diagram of this device is illustrated in Fig. 3.2. V_e is applied across cathode and anode, and the collector current, I_C, is measured across the n-Si. Due to the limitation of our deposition system, cathode and anode have a same kind of ferromagnetic material, CoFe. However, by depositing different thickness of CoFe in cathode and anode, the coercive fields of the cathode and anode are different, which causes a sharp change in collector current of spin valve measurement. The SBH of this device is determined by the interface between n-Si and Cu and is measured to be about 0.68eV. The surface preparation with HF etching and thin flim deposition in UHV enables a nearly ideal SBH between Cu and n-Si.

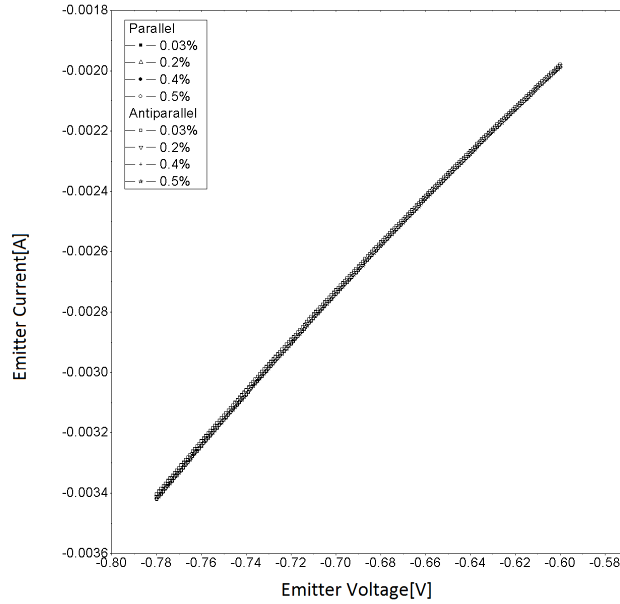

Figure 3.3: I_e as a function of V_e at different strains for parallel and anti-parallel magnetization. I_e is independent of strain and magnetization direction.

In order to find the exact magnetic field magnitude for I_P and I_{AP}, we measure I_C while sweeping the magnetic field at fixed V_e. The sign of magnetic field in Fig. 3.4 indicates the direction of the field. First, we apply high magnetic field in a negative direction and slowly change the magnetic field to the opposite direction. We apply sufficient V_e to inject electrons and a small V_C to allow electrons to drift across the n-Si. At the high magnetic field, the magnetization direction of two ferromagnetic materials are parallel, which corresponds to I_P. As the direction of the magnetic field changes to the opposite direction, the magnetization becomes anti-parallel, which reduces I_C. As explained in the previous chapter, the change of

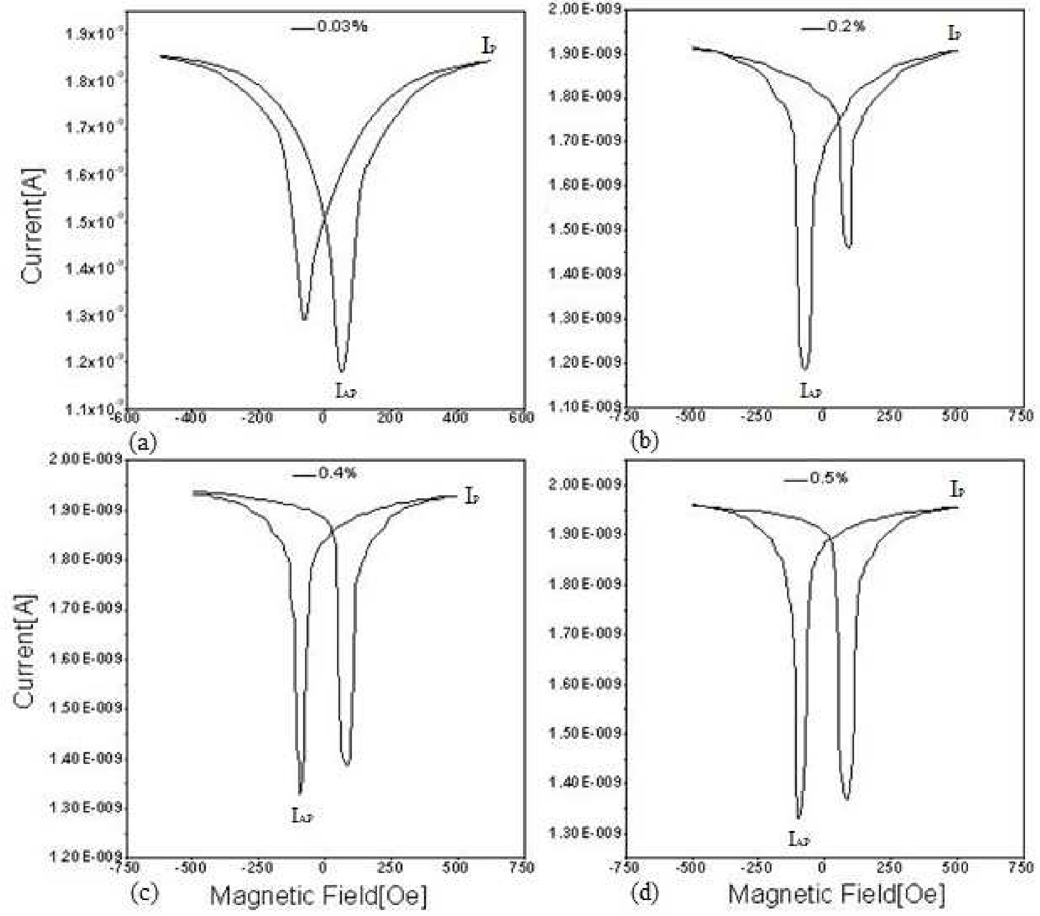

Figure 3.4: Spinvalve measurements at 115K. V_e is set at -0.78V for all plots. $I_P(I_{AP})$ in the plot indicates the parallel(anti-parallel) magnetization point of the magnetic field in order to measure Fig. 3.5 (a)Strain is set at 0.03%.(b) Strain 0.2%. (c) Strain 0.4%. (d) Strain 0.5%

.

I_C is very sharp as shown in Fig. 3.4. That is because the same kind of ferromagnetic material, CoFe, with different thickness is used in the cathode and anode, and the coercive fields are very close. The switching of magnetization directions of the cathode and anode occurs close the magnetic field sweep. Since the magnetic field range for I_{AP} is very narrow, it is important to find the exact point for I_{AP}, so near I_C minimum, we measured I_C with fine resolution in the magnetic field. I_P can be simply measured at a sufficiently high field. Each plot in Fig. 3.4 shows a spin valve measurement under different strains.

The electrical connection is shown in Fig. 3.2. The anode of tunnel junction is grounded. In Fig. 3.6, magnetoresistance (MR), which is a spin polarization, starts to be saturated near -0.78V. V_e applied in Fig. 3.4 is -0.78V. V_C is 0.2V in order to reduce the noise in I_C. To make contacts between the electrodes and the device, we have to apply a small strain around 0.03%. We measure the spin valve at various strains such as 0.03%, 0.2%, 0.4%, and 0.5%.

With exact magnetic field values for parallel(P) and anti-parallel(AP) magnetization, we measured SBH and MR with hot electron injection as a function of V_e. When V_e is far above the SBH, MR is saturated. For spin polarized hot electron injection, we varied V_e near the SBH from-0.60V to -0.78V. Also, in order to increase the signal to noise ratio, a small voltage, V_C, is applied across n-Si. In Fig. 3.5, I_C is measured as a function of V_e in P and AP magnetization. MR as a function of V_e is extracted from the I_C of P and AP with the equation, $P = \frac{I_P - I_{AP}}{I_P + I_{AP}}$. Note that in this experiment, depolarization of electron spin in silicon is not important. Electron spins are already filtered in P and AP magnetization before being injected into the

n-Si. Spin polarization in a 3 terminal device is independent of the silicon, because it only acts as a collector. In Fig. 3.5, I_P and I_{AP} near SBH, 0.68eV, increases exponentially with various strains such as 0.03%, 0.2%, 0.4%, and 0.5%. .

The primary purpose of this experiment is to test performance of tunnel junctions under high pressure. We successfully measured the spin valve effect under strain. Fig. 3.4 shows the spin polarized hot electron injection into silicon up to 0.5% strain. Since the spin polarized current comes from the tunnel junction, this is a clear evidence of the performance of tunnel junction under high pressure. Therefore, this verifies our ability to measure spin lifetime of uniaxially strained silicon.

Another purpose of this experiment is to measure the change of the SBH as a function of strain. However, due to the small signal near the SBH, the signal-to-noise ratio is too large to find its exact value. Even after smoothing and fitting the data, we could not determine the SBH. One source of noise comes from the method used to make electrical contacts to the device. The device and the electrode are compressed together to create electrical connections, which are less stable than directly wire bonding to the device. This experimental difficulty limits our measurement of the SBH. Due to small I_C of the devices below the SBH, the numerator and denominator of P becomes very small, which causes noise in the MR calculation as seen in Fig. 3.6.

We observe some interesting results in Fig. 3.4 and Fig. 3.6. In Fig. 3.4, we observe the change of the coercive field under different strain, so the magnetic field related to the I_{AP} changes with different strain. In Fig. 3.6, MR changes under different strains in the 3 terminal device. As strain increases, polarization increases

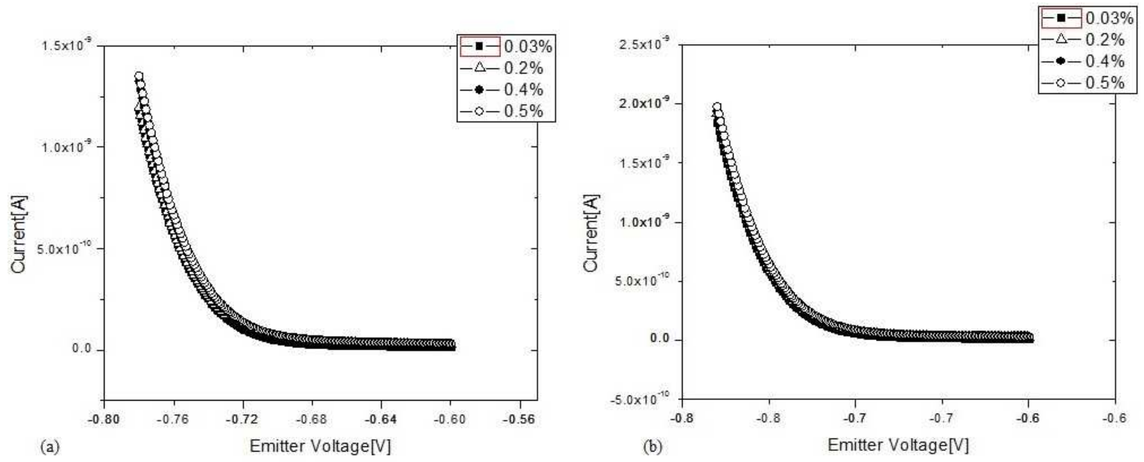

Figure 3.5: (a) Collector current I_C as a function of emitter voltage, V_e at 115K and V_C is 0.2V with anti-parallel magnetization directions of cathode and anode under various strains. (b) I_C as a function of V_e with parallel magnetization

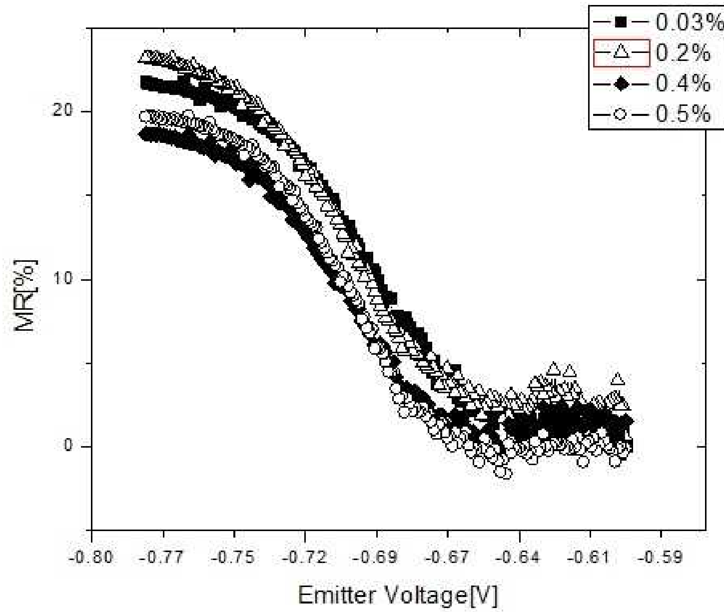

Figure 3.6: Magnetoresistance(MR) as a function of emitter voltage, V_e, near SBH at 115K. This is extracted from the I_P and I_{AP} in Fig. 3.5

up to a certain pressure, and then begins to decrease. As explained above, spin polarization in this device only depends on the ferromagnetic materials in cathode and anode. This change of polarization comes from the effects of strain on the ferromagnetic materials. This change of polarization happens when magnetizations are anti-parallel. In parallel case of Fig. 3.5(a), the change of I_C is small, which could be due to the change of the SBH. The lowering of the SBH increases I_C for a same V_e, but would not drastically change MR. This is consistent with an argument that the change of the spin polarization comes from the change in coercive fields of ferromagnetic materials.

Also, while measuring I_P and I_{AP} in Fig. 3.5 and Fig. 3.3, a characteristic I-V curves of the tunnel junction are measured from -0.60V to 0.78V. Fig. 3.3 shows that the tunneling current is independent from strain and magnetization direction, so Fig. 3.5 and Fig. 3.6 are not caused by strain induced changes to the tunnel junction.

By applying strain, magnetic domains in a ferromagnetic material in an external magnetic field can respond differently. Ferromagnetic materials are divided into small magnetic domains, each magnetic domain with its own magnetization direction. Without an external magnetic field, magnetic domains are randomly oriented, therefore, the bulk ferromagnetic material is not magnetized. However, in the presence of an external magnetic field, the spins in magnetic domains are aligned with the field. Strain-induced structural change of ferromagnetic materials causes the different responses to the external magnetic field. In other words, the local states of the ferromagnetic material are affected due to the structural change by strain.

That structural difference is why we can use same kind of ferromagnetic material in cathode and anode: Thickness dependent different domains create different coercive fields. One of the unique properties of ferromagnetic materials is magnetostriction. Magnetization due to the external magnetic field cause changes in shape or dimension of ferromagnetic materials, which can affect the coercive field. [35]. The opposite effect can occur. Strained ferromagnetic materials experience the change in their coercive fields. Magnetostrictive materials are used as a precise strain gauge. One experiment has already measured the change of coercive field due to strain by using magnetic tunnel junction (MTJ) [36]. This experiment employs an MTJ for a precise strain gauge has a very similar effect of the coercive field in strained ferromagnetic thin films. They used four point method to apply stable tensile and compressive strain to MTJ [37]. This explanation can be one of reasons for the shift of coercive field we observe in our spin valve measurements at various strains.

However, the above discussion is not enough to completely explain the measurements in Fig. 3.5 and Fig. 3.6. The I_P measured at different strains are almost same with slight increase due to the increase of carrier mobility and SBH lowering. On the other hand, I_{AP} in Fig. 3.5 (a) shows a larger difference under varying strain, so the change in I_{AP} due to strain causes the change in MR. MR under 0.03% strain is ∼22%. MR under 0.2% increases to ∼25%. As strain increases to 0.4%, MR decreases to ∼18%. Under 0.5% strain, MR remains at ∼ 20%. The complicated relationship of MR and strain is still ambiguous. This cannot be simply explained by strained thin ferromagnetic films. Another aspect of this device is the substrate. Ferromagnetic thin films are deposited on n-Si, where strain at the interface can play

a role in this change of MR. At the metal-semiconductor interface, there exists the depletion region caused by space charge effect, imaginary charges, and the charge neutrality which causes band bending of semiconductor [38]. Therefore, the conduction band and valence band are bent. In the case of n-Si, the Fermi level inside semiconductor should be flat throughout the material, so the distance between the Fermi level and conduction band increases closer to the interface.

In the case of vacuum-semiconductor junction, as the periodicity of the crystal structure is broken at the surface, at a few atomic layers at the surface, the change from the bulk material to vacuum causes the surface states to arise inside the band gap [39]. Similar phenomena occurs in the case of a metal-semiconductor junction. In 1947, John Bardeen introduced interface states inside the band gap of a semiconductor at the interface between semiconductor and metal [38], [40]. The metal and semiconductor junctions exhibit rectifying behavior or Schottky contacts due to the band bending [38]. Surface states are formed at the interface for various reasons such as dangling bonds and surface reconstruction, which are caused by chemical bonding between the metal and semiconductor, as well as defects on the surface, which already exists before the metal-semiconductor bonding. These surface states absorb the electrons from the metal. At the metal-semiconductor interface, the Fermi level at the surface is fixed close to the mid-band gap due to surface states and band bending, which is called Femi level pinning. In 1965, Volker Heine first explained that the tail end of electron wavefunctions in metal is extended into semiconductor. He explained the tails of the wavefunction behaves like localized surface states [41]. Dangling bonds are unpaired electrons in valence shells for covalent

bonds. These dangling bonds at the surface causes the shallow traps near valence band and conduction band so that these traps are hidden in valence and conduction bands [41]. Due to the Shockley theorem and dangling bonds, the surface states are stable for different kinds of metals on the semiconductor [41], [42]. Based on the Shockley theorem, the surface states are insensitive to the small changes in the boundary condition [42].

The MR changes as strain is applied to our device. This can be caused by the contribution of surface states. The strain can affect the extrinsic surface states at the interface between the anode and the n-Si. We inject spin polarized electrons into the conduction band of the silicon with the hot electron method. There are surface states near conduction band, which are called donor states. As explained in the Chapter 1, uniaxial strain induces repopulation between valleys and causes SBH lowering through the valley splitting. Since surface states also feel strain, we can induce a shift of surface states with strain. This shift of surface states and the conduction band can modify the coupling between conduction electrons and donor state electrons [43], [44]. If the donor states are unoccupied and the relaxation from conduction band to the donor states near conduction band minima depends on the spin state of conduction electrons, then the change of I_{AP} under various strains can be explained by the modification of surface states. This change of surface states can cause some difficulties to measure the exact SBH. The change of the MR as a function of V_e is not only induced by the hot electron injection method but also by a contribution of surface states to I_{AP}. Also, the change of the surface states is responsible for the same effects of thermal repopulation between valleys in silicon.

This leads us to think that surface states are also responsible for spin depolarization of hot electrons injection into silicon. Therefore, Fig. 3.6 cannot be explained by just one of these effects such as strained ferromagnetic films and strained silicon. The change of MR by strain in Fig. 3.6 can be the admixture of the change of coercive field of strained ferromagnetic films and the change of surface states in silicon. Also, even though we still have ambiguity in this measurement, we show the performance of tunnel junction under relatively high pressure.

Chapter 4: Conclusion

We demonstrate the spin polarized hot electron injection into silicon under uniaxial strain. The primary purpose of this experiment was to investigate the performance of tunnel junction under strain. We clearly show that thin films in a tunnel junction can survive under high pressure, which is one of the experimental challenges to measuring electron spin lifetime of silicon under strain. While testing the tunnel junction, we observed interesting strain effects on ferromagnet/silicon device. I_{AP} shows significant change under different strain is changed. We also provide some possible explanations for the change of MR and the coercive field due to strain. As discussed in the previous chapter, these can be induced by the modification of local states in ferromagnetic materials and the surface states at the interface between metal and silicon. This observation of the change of polarization in a tunnel junction device on n-Si due to strain needs to be studied further. This phenomena cannot be explained simply by one effect since it is caused by the competing effect of ferromagnetic materials and the interface between the metal and silicon. However, with our homemade strain probe to apply uniaxial pressure to a silicon device, the most challenging experimental issue of electron spin lifetime measurement in silicon is solved. The injection method of hot spin polarized electrons into silicon for the 4

terminal device is the same as in the 3 terminal device. We also show the design and the pictures of 4 terminal device and electrodes. The only configurational difference between 4 terminal and 3 terminal devices is only how we make electrically contacts to the device. As shown in Chapter 2, we can make good electrical contacts to the 4 terminal device. The magnitude of the current at the detector of a 4 terminal device is only hundreds of pico-Amps at the most. Since low signal-noise-ratio is very critical to a 4 terminal device measurement. Instead of compressing an electrode and a device, we connect a device to an electrode with a highly conductive silver paint and a small piece of indium in order to make solid electrical connections. Measuring spin lifetime of silicon with a 4 terminal device is already well studied as explained in the Chapter 1. We can extract electron spin lifetime in silicon from spinvalve measurements as a function of V_C which is a voltage-bias across i-Si. With this strain probe, we can apply various strains on devices at a low temperature. Therefore, even though more studies are needed with the 3 terminal device, we demonstrate a successful experimental method to measure conduction electron spin lifetime in uniaxially strained silicon at low temperature.

Bibliography

[1] Gary A Prinz. Magnetoelectronics. *Science*, 282(5394):1660–1663, 1998.

[2] SA Wolf, DD Awschalom, RA Buhrman, JM Daughton, S Von Molnar, ML Roukes, A Yu Chtchelkanova, and DM Treger. Spintronics: A spin-based electronics vision for the future. *Science*, 294(5546):1488–1495, 2001.

[3] Charles Kittel and Paul McEuen. *Introduction to solid state physics*, volume 7. Wiley New York, 1996.

[4] Daniel Loss and David P DiVincenzo. Quantum computation with quantum dots. *Physical Review A*, 57(1):120, 1998.

[5] Jaroslav Fabian, Alex Matos-Abiague, Christian Ertler, Peter Stano, and Igor Žutić. Semiconductor spintronics. *Acta Physica Slovaca. Reviews and Tutorials*, 57(4):565–907, 2007.

[6] Igor Žutić, Jaroslav Fabian, and S Das Sarma. Spintronics: Fundamentals and applications. *Reviews of modern physics*, 76(2):323, 2004.

[7] R. J. Elliott. Theory of the effect of spin-orbit coupling on magnetic resonance in some semiconductors. *Physical Review*, 96(2):266, 1954.

[8] Y Yafet. g factors and spin-lattice relaxation of conduction electrons. *Solid State Physics*, 14:1–98, 1963.

[9] Donald Long. Scattering of conduction electrons by lattice vibrations in silicon. *Physical Review*, 120(6):2024, 1960.

[10] Peter Y Yu and Manuel Cardona. *Fundamentals of semiconductors: physics and materials properties*. Springer Berlin etc, 1999.

[11] JL Cheng, MW Wu, and Jaroslav Fabian. Theory of the spin relaxation of conduction electrons in silicon. *Physical review letters*, 104(1):016601, 2010.

[12] Jing Li. *Extrinsic spin relaxation in silicon spin transport devices*. PhD thesis, University of Delaware, 2012.

[13] Yang Song and Hanan Dery. Analysis of phonon-induced spin relaxation processes in silicon. *Physical Review B*, 86(8):085201, 2012.

[14] Pengke Li and Hanan Dery. Spin-orbit symmetries of conduction electrons in silicon. *Physical Review Letters*, 107(10):107203, 2011.

[15] Jing Li, Lan Qing, Hanan Dery, and Ian Appelbaum. Field-induced negative differential spin lifetime in silicon. *Physical Review Letters*, 108(15):157201, 2012.

[16] Enzo Ungersboeck, Siddhartha Dhar, Gerhard Karlowatz, Viktor Sverdlov, Hans Kosina, and Siegfried Selberherr. The effect of general strain on the band structure and electron mobility of silicon. *Electron Devices, IEEE Transactions on*, 54(9):2183–2190, 2007.

[17] Martin M Rieger and P Vogl. Electronic-band parameters in strained $\mathrm{si}_{1-x}\mathrm{ge}_x$ alloys on $\mathrm{si}_{1-y}\mathrm{ge}_y$ substrates. *Physical Review B*, 48(19):14276, 1993.

[18] Hiroshi Hasegawa. Theory of cyclotron resonance in strained silicon crystals. *Physical Review*, 129(3):1029, 1963.

[19] Marius Grundmann. *The Physics of Semiconductors: An Introduction Including Nanophysics and Applications*. Springer, 2011.

[20] Jian-Ming Tang, Brian T Collins, and Michael E Flatté. Electron spin-phonon interaction symmetries and tunable spin relaxation in silicon and germanium. *Physical Review B*, 85(4):045202, 2012.

[21] Athanasios Dimoulas. *Advanced gate stacks for high-mobility semiconductors*, volume 27. Springer, 2007.

[22] Hanan Dery, Yang Song, Pengke Li, and Igor Zutic. Silicon spin communication. *Applied Physics Letters*, 99(8):082502–082502, 2011.

[23] Srijit Goswami, KA Slinker, Mark Friesen, LM McGuire, JL Truitt, Charles Tahan, LJ Klein, JO Chu, PM Mooney, Daniel W Van Der Weide, et al. Controllable valley splitting in silicon quantum devices. *Nature Physics*, 3(1):41–45, 2006.

[24] Ian Appelbaum, Biqin Huang, and Douwe J Monsma. Electronic measurement and control of spin transport in silicon. *Nature*, 447(7142):295–298, 2007.

[25] Joachim Kessler. *Polarized electrons*, volume 1. Springer, 1985.

[26] Biqin Huang, Douwe J Monsma, and Ian Appelbaum. Coherent spin transport through a 350 micron thick silicon wafer. *Physical Review Letters*, 99(17):177209, 2007.

[27] C Canali, C Jacoboni, F Nava, G Ottaviani, and A Alberigi-Quaranta. Electron drift velocity in silicon. *Physical Review B*, 12(6):2265, 1975.

[28] H. Kroemer. Theory of the gunn effect. *Proc. IEEE*, 52:1736, 1964.

[29] ED Marquardt, JP Le, and Ray Radebaugh. Cryogenic material properties database. In *Cryocoolers 11*, pages 681–687. Springer, 2002.

[30] Chun-Hyung Cho. Characterization of youngs modulus of silicon versus temperature using a beam deflection method with a four-point bending fixture. *Current Applied Physics*, 9(2):538–545, 2009.

[31] B Welber, CK Kim, Manuel Cardona, and Sergio Rodriguez. Dependence of the indirect energy gap of silicon on hydrostatic pressure. *Solid State Communications*, 17(8):1021–1024, 1975.

[32] P Kramer and LJ Van Ruyven. Position of the band edges of silicon under uniaxial stress. *Applied Physics Letters*, 20(11):420–422, 1972.

[33] Michel Julliere. Tunneling between ferromagnetic films. *Physics Letters A*, 54(3):225–226, 1975.

[34] Shinji Yuasa, Taro Nagahama, Akio Fukushima, Yoshishige Suzuki, and Koji Ando. Giant room-temperature magnetoresistance in single-crystal fe/mgo/fe magnetic tunnel junctions. *Nature materials*, 3(12):868–871, 2004.

[35] James Prescott Joule. Xvii. on the effects of magnetism upon the dimensions of iron and steel bars. *The London, Edinburgh, and Dublin Philosophical Magazine and Journal of Science*, 30(199):76–87, 1847.

[36] M Lohndorf, T Duenas, M Tewes, E Quandt, M Ruhrig, and J Wecker. Highly sensitive strain sensors based on magnetic tunneling junctions. *Applied physics letters*, 81(2):313–315, 2002.

[37] M Lohndorf, TA Duenas, Alfred Ludwig, M Ruhrig, J Wecker, D Burgler, P Grunberg, and Eckhard Quandt. Strain sensors based on magnetostrictive gmr/tmr structures. *Magnetics, IEEE Transactions on*, 38(5):2826–2828, 2002.

[38] J Tersoff. Schottky barrier heights and the continuum of gap states. *Physical Review Letters*, 52(6):465–468, 1984.

[39] G Sydney and Maria Stęślicka. *Basic theory of surface states*, volume 46. Oxford University Press, 1996.

[40] Winfried Mönch. *Semiconductor surfaces and interfaces*, volume 26. Springer, 2001.

[41] John Bardeen. Surface states and rectification at a metal semi-conductor contact. *Physical Review*, 71(10):717, 1947.

[42] Volker Heine. Theory of surface states. *Physical Review*, 138(6A):A1689, 1965.

[43] William Shockley. On the surface states associated with a periodic potential. *Physical review*, 56(4):317, 1939.

[44] DK Wilson and G Feher. Electron spin resonance experiments on donors in silicon. iii. investigation of excited states by the application of uniaxial stress and their importance in relaxation processes. *Physical Review*, 124(4):1068, 1961.